Microporous and Mesoporous Materials 158 (2012) 219–228

Contents lists available at SciVerse ScienceDirect

Microporous and Mesoporous Materials

journal homepage: www.elsevier.com/locate/micromeso

Sorption and kinetics of CO_2 and CH_4 in binderless beads of 13X zeolite

José A.C. Silva [a,*], Kristin Schumann [c], Alírio E. Rodrigues [b]

[a] Escola Superior de Tecnologia e Gestão, Instituto Politécnico de Bragança, Apartado 134, 5301-857 Bragança, Portugal
[b] Laboratory of Separation and Reaction Engineering, Departamento de Engenharia Química, Faculdade de Engenharia, Universidade do Porto, Rua do Dr. Roberto Frias s/n, Portugal
[c] Chemiewerk Bad Köstritz GmbH, Heinrichshall 2, 07586 Bad Köstritz, Germany

ARTICLE INFO

Article history:
Received 17 February 2012
Received in revised form 18 March 2012
Accepted 22 March 2012
Available online 30 March 2012

Keywords:
Binderless 13X zeolite
Sorption of CO_2/CH_4
ZLC technique
Adsorption equilibrium

ABSTRACT

The sorption equilibrium of CO_2 and CH_4 in binderless beads of 13X zeolite has been investigated between 313 and 373 K and pressure up to 4 atm. The amount adsorbed of CO_2 and CH_4 is around 5.2 mmol/g_{ads} and 1.2 mmol/g_{ads}, respectively, at 313 K and 4 atm. Comparing these values with the ones in literature the value of CO_2 is 20% higher than in CECA 13X binder pellets. It is also found that isotherms are pronounced Type I for CO_2 and almost linear for CH_4. The CO_2 isotherms were modeled using a simple deviation from Langmuir isotherm that takes into account interaction between adsorbed molecules at adjacent sites (Fowler model) suggesting a moderate repulsion. Henry's constants range from 143 to 11.1 mmol/g_{ads}.atm for CO_2 and 0.45 to 0.27 mmol/g_{ads}.atm for CH_4 between 313 and 373 K, respectively. The heats of sorption at zero coverage are 43.1 kJ/mol for CO_2 and 9.2 kJ/mol for CH_4.

The sorption kinetics has been investigated by the Zero-Length Column technique (ZLC). Recipes to analyze ZLC desorption curves in pellets of adsorbents are reviewed and it is derived a criteria which indicates that for the sorption rate be measured macroscopically the time of the experiment (that should be above a few seconds) is directly calculated with the following expression: $t_{0.1} \geq 7.02 \times 10^{-2} \frac{r_c^2}{D_c}$. Based on such criteria it is shown that crystal diffusivity of CO_2 in 13X can be measured macroscopically by ZLC, being the same measurement for CH_4 practically impossible. The crystal diffusivity of CO_2 measured experimentally is 5.8×10^{-15} m^2/s and 1.3×10^{-15} m^2/s at 373 and 313 K, respectively. These values are comparable to the ones measured by a frequency response and pulse chromatography techniques reported in literature. The ZLC desorption curves for CH_4 were measured under an equilibrium regime.

1. Introduction

The reduction of carbon dioxide and methane emissions to atmosphere is a matter of great concern nowadays since both gases can contribute significantly to the so-called greenhouse effect that describes the trapping of heat near earth's surface by gases in the atmosphere. Indeed, carbon dioxide is necessary because there are calculations showing that if it were not present in the atmosphere earth will be 30 °C cooler. The presence of CO_2 in the atmosphere is ruled by the carbon cycle but today that balance has probably been upset. At the same time CO_2/CH_4 separations are of great economical and technological importance in treating gas streams like landfill gas, biogas and coal-bed methane. Accordingly, there is a need to investigate on this topic and that can be done with improved efficient technologies to separate or remove CO_2 and CH_4 from exhaust gases.

Two recent reviews discuss this matter with great detail concerning the use of adsorbent based techniques to handle CO_2 capture and CO_2/CH_4 separations [1,2]. A new class of adsorbents named Metal–Organic Frameworks (MOFs) are focused being clear that in future they can be an excellent alternative to zeolite adsorbents generally used nowadays. However, MOFs need to be further refined regarding its production in large scale, chemical and thermal stability, which are properties already well-established in zeolites.

There are today adsorption processes based in zeolites like Pressure Swing Adsorption – PSA to store and separate compounds such as CO_2 and CH_4. To be used as adsorbents zeolite powder needs to transformed into molecular sieves and this reduces its working capacity in 20% or more which is the amount of adsorptive inert clay binder generally used to give the necessary mechanical strength to the pellets or beads in order to be used in packed-columns and at the same time reduce pressure drop. To increase the working capacity the binder can also be converted to zeolite matter leading to the so-called binderless pellets or beads [3,4] but this technology has not received great attention from companies that produce molecular sieves. Recently, this technology has been recovered and applied for the synthesis of binderless beads of 13X zeolite where the non-zeolitic components (temporary binder) is converted to zeolite during a hydrothermal conversion after the manufacturing procedure [5]. The resulting binderless beads can

* Corresponding author. Tel.: +351 273 30 3125.
E-mail address: jsilva@ipb.pt (J.A.C. Silva).

1387-1811/$ - see front matter © 2012 Elsevier Inc. All rights reserved.
http://dx.doi.org/10.1016/j.micromeso.2012.03.042

Nomenclature

b	isotherm equilibrium constant, Pa^{-1}
c	outlet concentration of the ZLC, mol/m^3
c_0	saturation concentration of the ZLC, mol/m^3
D_c	crystal diffusivity, m^2/s
D_p	macropore diffusivity, m^2/s
D_m	molecular diffusivity, m^2/s
D_K	Knudsen diffusivity, m^2/s
F	purge flowrate n ZLC, m^3/s
H	Henry's law, mol/g.Pa
K	adsorption equilibrium constant (Henry's law constant), dimensionless
L	ZLC model parameter, dimensionless
p	pressure, Pa^{-1}
q	amount adsorbed, mol/kg
q_m	amount adsorbed at the saturation of the adsorbent, mol/kg
r_c	crystal radius, m
R_p	pellet radius, m
w	is the extra energy (Fowler isotherm), J/mol
R	ideal gas constant, J/mol.K
t	time, s
T	temperature, K
V_s	volume of adsorbent, m^3
R_p	pellet radius, m

Greek symbols

ρ_p	pellet density, kg/m^3
ε_p	pellets porosity. Dimensionless
Γ_p	tortuosity, dimensionless
β_1	roots of transcendental Eq. (4), dimensionless
θ	coverage equal to q/q_m; the same as degree of filling of sites, dimensionless

increase in this way the working capacities of existing zeolite adsorbent technologies.

In literature we can find several data and modeling regarding the sorption of CO_2 and CH_4 in zeolites [6–10] and MOFs [11–17]. Among the zeolites one of the most interesting is zeolite 13X due to its large cages that can accommodate a large amount of mass and at the same time the presence of cations that produce electric field that interacts with strong quadropole moment molecules such as CO_2. This gives rise to an increased selectivity between CH_4 (apolar) and CO_2 that has been exploited in cyclic processes [18–21].

For the modeling of adsorption processes it is of fundamental importance to analyze conveniently thermodynamic data. The books of Barrer [22], Ruthven [23], Guiochon et al. [24] and Do [25] highlight in great detail the basics to analyze such data. For Type I isotherms which are the most frequent in zeolites, localized adsorption models such as: Langmuir, dual-site-Langmuir, Fowler, Nitta, etc. are used extensively due to their simplicity and at the same time being thermodynamic consistent giving insight into sorption events in a comprehensive way.

The measurement of sorption kinetic is also fundamental for modeling adsorption cyclic processes since the transport of mass into and out of the adsorbent can affect significantly the performance of industrial processes. For the measurement of sorption kinetics there are several techniques, one is microscopic (PFG, NMR) and the other is macroscopic (uptake rate, chromatographic) [26–28]. Since its introduction by Eic and Ruthven [29] for the measurement of intracrystalline diffusivities in strongly adsorbed species the Zero-Length Column (ZLC) technique has been used extensively for the measurement of sorption rates in porous media due to its apparent simplicity [30–33]. However, special attention in the use of model parameters from which kinetic data are obtained is required since there are models with the same mathematical form in completely different regimes that when used without previous calculations can produce erroneous results [34]. Extensions for using the technique for liquid systems [35,36], pellets of adsorbents [37], analyses of influence of heat effects [38,39], effect of non-linear equilibrium [40], effect of surface barriers [41,42] and also for the measuring of adsorption equilibria have been developed [43], being now possible to use the technique in a broad range of systems sorbate-sorbent.

The goal of this work is to access data of equilibrium and kinetics of sorption of CO_2 and CH_4 on a new type of binderless beads of 13X zeolite. The equilibrium data are measured in a breakthrough apparatus and the kinetic data by the ZLC technique.

Attention is made regarding the comparison of these results with published data on pellets of the same zeolite type with binder. At the same time thermodynamic and kinetic parameters are obtained that are useful for the development of adsorption separation processes such as the ones calculated from modeling of equilibrium and kinetic of sorption: heats of sorption, Henry's constants, equilibrium constants, working capacities, inter and intracrystalline diffusivities. Through this work some ideas about the use ZLC technique for the measurement the diffusivity in porous adsorbents are revised by establishing a procedure to analyse properly such results introducing a simple criteria to evaluate which kind of systems can be measured macroscopically by ZLC.

2. Experimental section

2.1. Binderless 13X zeolite

The powder of 13X from which the binderless beads were formed is from Chemiewerk Bas Kostritz GmbH (Germany) with a Si/Al ratio of 1.18. Metakaolin is used to manufacture the beads. The synthesis and characterization procedure is described in detail elsewhere [5]. Briefly, the beads formed consist in spherical particles with a diameter ranging from 1.2 to 2.0 mm. The size of the zeolite crystals are around 2 μm. Table 1 summarizes the characteristics of the beads.

2.2. Adsorption equilibrium and ZLC apparatus

The equilibrium and kinetics studies were performed in the apparatus illustrated in Fig. 1. Briefly, it consists in two sections: i) a gas preparation system; and ii) a Gas Chromatograph with a

Table 1
Physical properties of zeolite 13X beads and adsorption column characteristics.

Physical properties of binderless 13X beads[a]	
SiO_2/Al_2O_3 ratio	2.35
Crystal dimensions (μm)	≈2
Beads dimension (spherical) (mm)	1.2–2.0
Average pore diameter (μm)	0.6
Adsorption column characteristics	
Length (cm)	8
Internal diameter (mm)	4.6

[a] From Ref. [5].

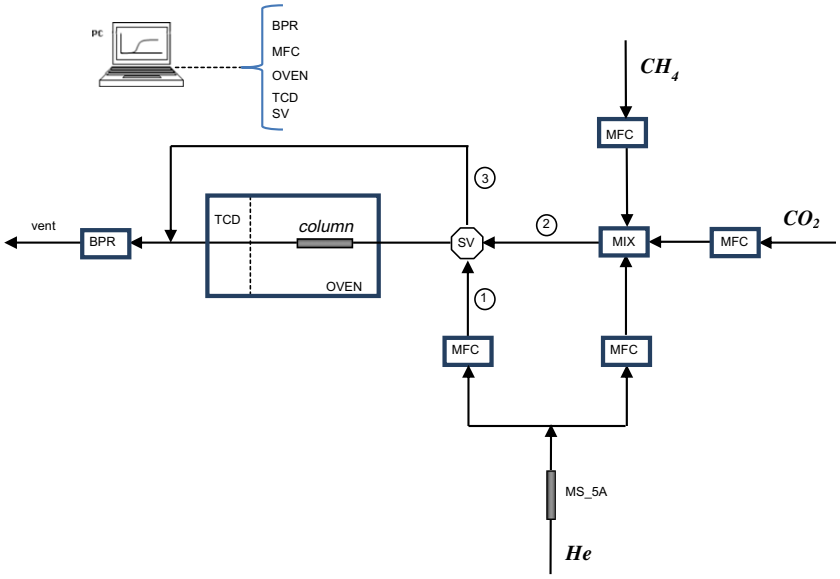

Fig. 1. Schematic diagram the experimental apparatus used to measure adsorption equilibrium and ZLC data: (Column) Adsorption column; (TCD) detector of chromatograph; (MFC) mass flow controller; (PC) computer; (SV) 5-way crossover valve; (BPR) back-pressure regulator; (①②③) streams.

TCD detector where the adsorption column is placed. In the gas preparation section it is used helium as the inert gas which is previously dehydrated in a molecular sieve type 5A. Helium enters in the system by two different streams: one line to be mixed with sorbate species (CO_2 and CH_4) and the other where it is pure (line 1).

The He from line (1) and the mixture (sorbate + inert) from line (2) run to a 6-way crossover valve (SV) that allows the selection of which line 1 or 2 passes by the adsorption column. The line that does not enter in the adsorption column is by-passed through line 3. The pressure of all the system is controlled by a back-pressure-regulator (BPR). The effluent of the adsorption column passes directly by the reference side of a TCD that can detect concentration of all gases to around 100 ppm (if needed a part of this effluent could by-pass the TCD).

The adsorption column consists of a 4.6 mm i.d. stainless steel column with 80 mm length. For the adsorption equilibrium studies the column is entirely filled with zeolite beads. In ZLC experiments just the bottom of the column is filled with few adsorbent particles, being the remaining space occupied with small glass spheres. Valve position, oven temperature, mass flows, back-pressure regulator and TCD signal are completely automated.

The sorbate and inert gases were furnished by air liquid with the following purities: methane N35 (99.95%), carbon dioxide N48 (99.998%), and helium ALPHAGAZ 2 (99.9998%)

2.3. Procedure for sorption equilibrium experiments

Before time zero of an experiment the switch valve (SV) directs pure helium that flows through line 1 to the adsorption column, and vent through line 3 the mixture that comes from line 2 prepared by a combination of mass flows of sorbate plus helium. At time zero switch valve (SV) is switched allowing line 2 to enter in the column venting at the same time line 1. The experiment consists in measuring continuously the concentration as a function of time at the outlet of the bed by the TCD. The equilibrium loading of the experiment is obtained by integrating the concentration profiles of the breakthrough curve with a procedure described elsewhere [44]. Before the first run the adsorption column is activated for at least 24 h at 493 K under pure helium flow. When the adsorption experiment finishes SV is switched again. Once the TCD signal reaches its lower level another run is performed. One run means one equilibrium point of the isotherm.

2.4. Procedure for ZLC experiments

For the ZLC experiments we follow strictly the guidelines provided by Eic and Ruthven in the original ZLC paper [29]. Especially: 1) Set-up a low concentration of sorbate to validate Henry's law of isotherm; 2) Blank runs to account for extraneous capacities (no-problems were found since in our system the column is directly attached to the detector); 3) Perform experiments with different purge flowrates to see the proportionality between parameter L and the flowrate. 4) set-up a differential bed (50 mg of pellets were used in the experiments).

The ZLC experiment is similar to the one performed for the adsorption equilibrium measurements. Before time zero SV directs the flow of line 2 (which contains a very low concentration of the sorbate species around 0.01 atm) to the column. At time zero SV is switched and line 1 (pure helium) is allowed to pass through the adsorption column initiating the desorption curve. The signal produced by the TCD is continuously monitored by a computer for future data treatment in order to set-up of the desorption curve in terms of concentration *versus* time.

3. Theoretical

3.1. Pure components isotherms

A simple and suitable model to represent type I isotherms is the Langmuir equation:

$$\frac{1}{p}\frac{\theta}{(1-\theta)} = b \tag{1}$$

where $\theta = q/q_m$ is the degree of filling of sites, b is an equilibrium constant, p the pressure, q the amount adsorbed and q_m is the amount adsorbed at the saturation of the adsorbent. The Langmuir equation is perfect to represent sorption in a homogeneous sites surface where a sorbate molecule occupies one active site when it adsorbs with no interaction between adsorbed molecules.

To account for lateral interactions between adsorbed molecules Fowler [45] proposed the following equation

$$\frac{1}{p}\frac{\theta}{(1-\theta)} = b\exp(-2w\theta/RT) \tag{2}$$

where w is the extra energy when sorbate molecules occupy adjacent sites (positive for repulsion, negative for attraction), R the ideal gas constant and T the temperature.

The validity of both models can be easily verified by plotting $\log\frac{1}{p}\frac{\theta}{(1-\theta)}$ against θ. If we find a horizontal line the Langmuir model is valid. In the case of Fowler isotherm equation we will find a straight line with slope $-2w/RT$. To better test both models it is convenient to know a priori the parameter q_{max} but it can be relaxed during verification if no data are known.

3.2. ZLC models

The Zero-Length Column (ZLC) technique [29] for measuring diffusivites in adsorbents consists in a differential bed of porous particles that is first saturated with the sorbate species preferably at a very low concentration under the validity of the Henry's law of the isotherm. At time zero the carrier gas (free of sorbate) flows through the ZLC and the desorption curve is measured as a function of time.

As explained by Eic and Ruthven model parameters can be easily obtained using the information of desorption curves at long times. The model of the ZLC based on the Ficks law of diffusion reduces at long times to the following linear equation in a semi-log plot,

$$\ln\left(\frac{c}{c_0}\right) = \ln\left(\frac{2L}{\beta_1^2 + L(L-1)}\right) - \beta_1^2 \frac{D_c}{r_c^2} t \tag{3}$$

where,

$$\beta_1 \cot(\beta_1) + L - 1 = 0 \tag{4}$$

$$L = \frac{1}{3}\frac{F}{KV_s}\frac{r_c^2}{D_c} \tag{5}$$

In the previous equations c is the outlet concentration of the ZLC, c_0 is the saturation concentration, t is the time, β_1 are the roots of transcendental Eq. (4), D_c is the crystal diffusivity, r_c the crystal radius, L a model parameter, F the purge flowrate, V_s the volume of adsorbent and K a dimensionless adsorption equilibrium constant (Henry's law constant). The previous model is valid for the measurement of intracrystalline diffusivity. If experiments are made in pellets and if the controlling mechanism of diffusion is the one in the macropores of the pellets the previous equations are slightly modified being,

$$\ln\left(\frac{c}{c_0}\right) = \ln\left(\frac{2L}{\beta_1^2 + L(L-1)}\right) - \beta_1^2 \frac{D_p}{R_p^2(1+K)} t \tag{6}$$

$$L = \frac{1}{3}\frac{F}{V_s}\frac{R_p^2}{D_p} \tag{7}$$

where D_p is the macropore diffusivity and R_p is the pellet radius. Considering that diffusion in macropores is Knudsen diffusivity in series with molecular diffusion, the pore diffusivity can be estimated by,

$$D_p = \frac{1}{\Gamma_p\left(\frac{1}{D_m} + \frac{1}{D_K}\right)} \tag{8}$$

where Γ_p is the tortuosity, D_m is the molecular diffusivity and D_K is the Knudsen diffusivity.

If experiments in ZLC are performed under an equilibrium regime $L < 0.1$ the previous equations can be substituted with the following equation [43],

$$\ln\left(\frac{c}{c_0}\right) = -\frac{F}{kV_s} t. \tag{9}$$

Recipes for using ZLC technique carefully are given comprehensively and with great detail in the original paper by Eic and Ruthven [29].

4. Results and discussion

4.1. Sorption isotherms

The experimental single component sorption isotherms measured for CO_2 and CH_4 in 13X are shown in Fig. 2a and b, respectively. Data were collected at three temperatures: 313, 343 and 373 K and for partial pressures (helium as inert) up to 4 atm. We can observe in Fig. 2 that CH_4 isotherms are practically linear and marked type I for CO_2 in the range of temperature and pressure studied. As expected [6,9,10], Fig. 1 shows that CO_2 is the more strong adsorbed component with an amount adsorbed that reaches more than 5 mmol/g_{ads} at 313 K and partial pressure around 4 atm. For the same pressure and temperature the amount adsorbed of CH_4 is much smaller being almost 1.2 mmol/g_{ads}. This means also a selectivity CO_2/CH_4 around 4.2. Since we use binderless beads it is expected that the sorption capacity increases, being of interest to compare our data with 13X zeolite with binder. Looking at data measured by Mulgundmath et al. [9] in CECA 13X zeolite of mesh size 20–60 our data compares to 4.0 mmol/g_{ads} for CO_2 and 1.27 mmol/g_{ads} for CH_4. Regarding the data on CECA 13X extrudates of 1.6 mm [10] the data of the present work compares to

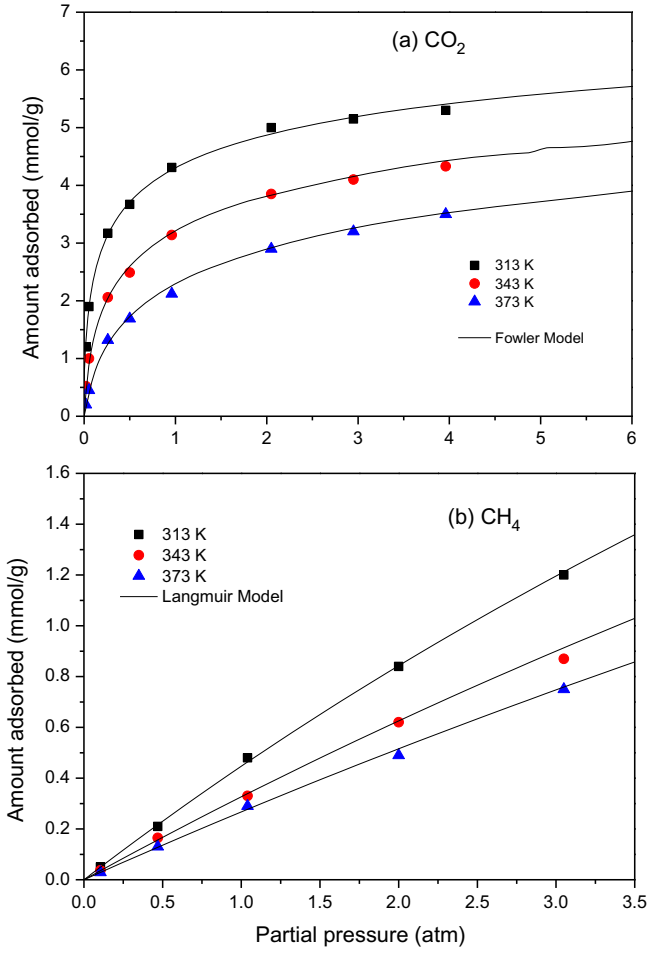

Fig. 2. Adsorption equilibrium isotherms of CO_2 and CH_4 on binderless 13X zeolite. (a) CO_2, (b) CH_4. Temperatures are quotes in each curve. Points are experimental data and lines model predictions.

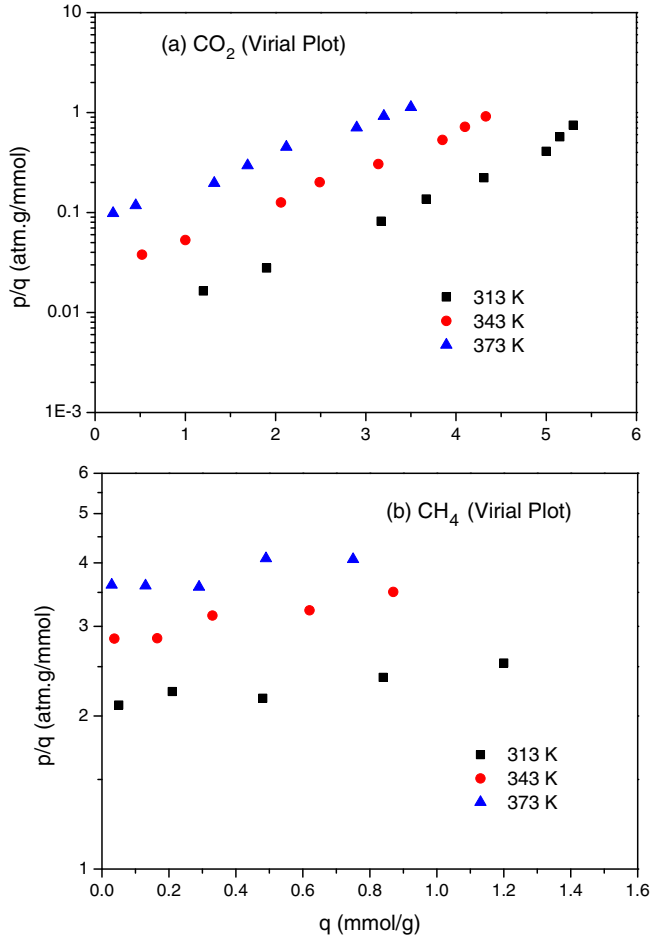

Fig. 3. Semi-log plots of p/q *vs.* q for analysis of virial isotherm in binderless 13X zeolite (a) CO_2, (b) CH_4.

4.05 mmol/g for CO_2 at 308 K and 1.32 mmol/g for CH_4 at 308 K. This means that the binderless 13X studied in this work increases the sorption capacity in 20% for CO_2 being the values for CH_4 practically the same.

To calculate directly Henry's constants from experimental data we plot *p/q versus p* according to a Virial Plot. Extrapolation of data to zero coverage gives us the reciprocal of Henry's constants. Fig. 3 shows such plots in semi-log coordinates for both CO_2 and CH_4 and Table 2 the calculated values. For CO_2 the Henry's constants range from 143 to 11.1 mmol/g_{ads}.atm between 313 and 373 K, respectively. These very high values are clearly due to the strong bonds between CO_2 and the cations of zeolite in spite of the large quadropole moment of CO_2. For CH_4 the values are much smaller and range between 0.45 to 0.27 mmol/g_{ads}.atm in the same temperature interval level. As a result, we found that the selectivity CO_2/CH_4 at low partial pressure measured by the ratio of the Henry's constants at 313 K is 143/0.45 equal to 318. This is a very high value.

To model sorption data we decided to use localized adsorption models where the Langmuir model is the simpler one. Fig. 4 shows

Table 2
Isotherm model parameters for sorption of CO_2 and CH_4 in binderless beads of 13X zeolite.

Isotherm models		CO_2 Fowler	CH_4 Langmuir
q_m	(mmol/g_{ads})	7.4[a]	7.4[a]
$-\Delta H$	(kJ/mol)	43.1	9.2
w	(kJ/mol)	6.1	–
313 K			
H[b]	(mmol/g_{ads}.atm)	143	0.45
b	(atm^{-1})	21.3	0.0643
343 K			
H[b]	(mmol/g_{ads}.atm)	38.5	0.34
b	(atm^{-1})	4.76	0.0462
373 K			
H[b]	(mmol/g_{ads}.atm)	11.1	0.27
b	(atm^{-1})	1.49	0.0374

[a] From Ref. [2,10].
[b] Henry's constant calculated from Virial plots.

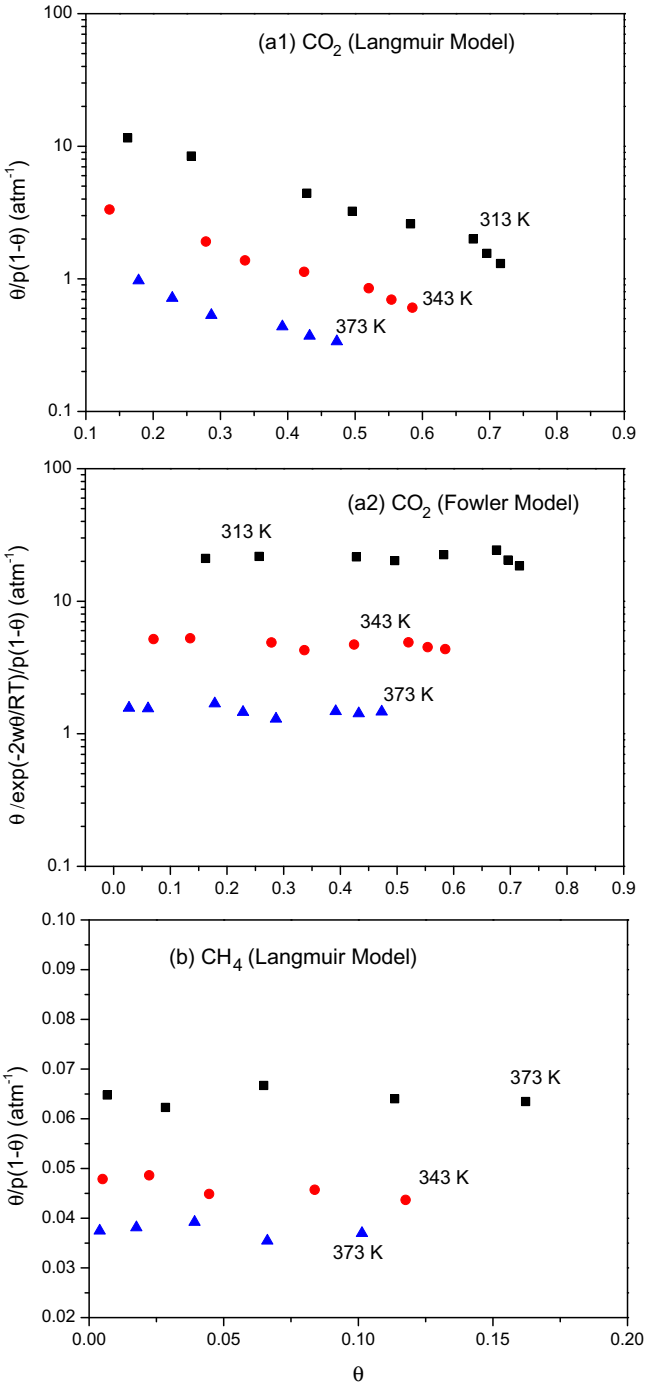

Fig. 4. Semi-log plots of $\theta/p(1-\theta)$ or $\theta/\exp(-2w/RT)/p(1-\theta)$ against θ for the binderless 13X zeolite studied in this work. (a1) CO_2 (Langmuir model); (a2) CO_2 (Fowler model); (b) CH_4 (Langmuir model).

a semi-log plot of $\theta/p(1\text{-}\theta)$ against θ for both components for the data measured in this work. In Fig. 4a1 we see such plot for CO_2 and in Fig. 4b for CH_4. For the representation we use a maximum adsorbed quantity (q_{max}) for CO_2 in 13X taken from literature of 7.4 mmol/min [2,10]. It is clear from Fig. 4a1 that for CO_2 the Langmuir model is not valid since we do not see a linear representation of data parallel to the axis of θ. In contrary we observe a decay of data with a linear slope suggesting that Fowler model that accounts for interactions between adsorbed molecules is valid. To confirm if Fowler model represent CO_2 sorption in 13X we plot in Fig. 4a2 $\theta/p(1-\theta)\exp(-2w/RT)$ against θ according to Eq. (2) keeping the same value of q_{max}. Choosing a value of w equal to 6.1 kJ/mol we obtain a plot where data is linear and parallel to the axis of θ validating Fowler model. It should be noted that if we choose a lower q_{max} that will be reflected in the value of w that will also decrease. The value for w of 6.1 kJ/mol suggests a moderate repulsion between adsorbed molecules in adjacent sites. For the case of CH_4 it is clearly seen in Fig. 4b that Langmuir model is valid with no need to account for lateral interactions between adsorbed molecules.

Fig. 5 shows the effect of loading on the isosteric heat of sorption for CO_2 and CH_4 (calculated from a plot lnP *vs* $1/T$ at constant loading). In Fig. 5 we can observe a linear decrease of the isosteric heat of sorption with loading for CO_2 being the isosteric heat practically constant for CH_4. The linear increase or decrease of the heat of sorption with coverage can be predicted by the Fowler isotherm depending of the value of parameter w [25]. If interaction energies are attractive w is negative and we will observe a linear increase of the heat with coverage. On the contrary if w is positive interaction energies are repulsive and the heat of sorption will decrease linearly with coverage. For the present study we observe a linear decrease of the heat of sorption with coverage since parameter w is positive. The decrease of the heat of sorption with coverage for quadropolar CO_2 in several adsorbents has been already reported by Barrer and Ruthven [22,23] and is attributed to polarizing effects between cations in the framework and CO_2 leading to energetic heterogeneity of sites. In the present case, the balance between adsorbate–adsorbent and adsorbate–adsorbate interactions energies is clearly lumped in parameter w and consequently in the exponential of Fowler isotherm leading to experimental observed behavior.

To confirm if Fowler isotherm can give a description of the sorbate-sorbent system under study in a broad range of pressure and temperature, we apply the same procedure for the data measured in 13X CECA pellets by Cavenati et al. [10] between 298 K and 323 K and pressures until 30 atm. Fig. 6 shows in a semi-log plot $\theta/p(1\text{-}\theta)$ against θ such data, keeping the maximum amount adsorbed close to 7.4 mmol/g_{ads} for CO_2 and CH_4. In Fig. 6a1 and b we can observe a similar trend of the one shown in Fig. 4 indicating that for CO_2 there is a sorbate–sorbate interaction for CO_2 being the same type of interaction for CH_4 practically inexistent. In Fig. 6a2 we plot $\theta/p(1-\theta)\exp(-2w/RT)$ against θ using the previous value of w equal to 6.1 kJ/mol and it was found that until very near the saturation of the adsorbent Fowler isotherm is capable to describe the sorption behavior of CO_2 and Langmuir isotherm for CH_4. When

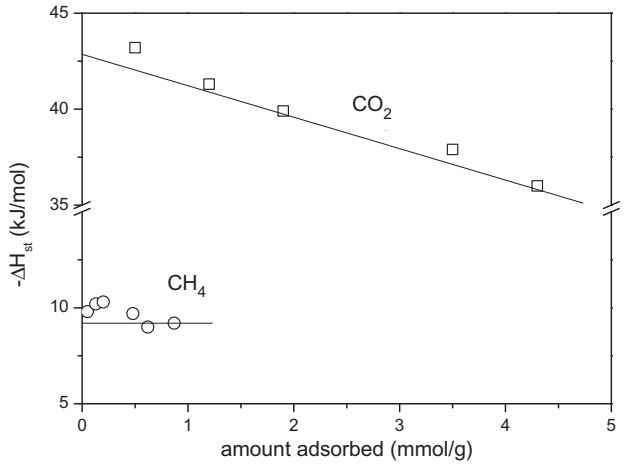

Fig. 5. Isosteric heat of adsorption as function of amount adsorbed. Points are experimental data and lines model predictions for CO_2 (Fowler model) and CH_4 (Langmuir model).

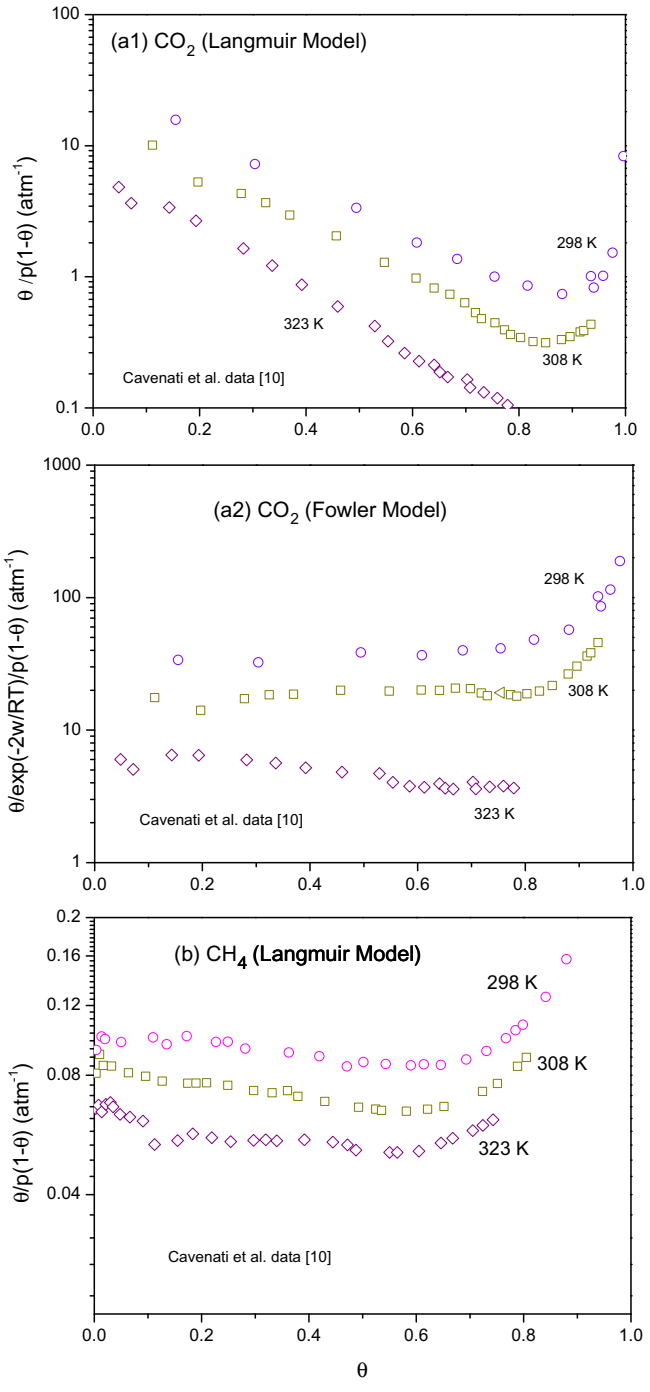

Fig. 6. Semi-log plots of $\theta/p(1\text{-}\theta)$ or $\theta/\exp(-2w/RT)/p(1\text{-}\theta)$ against θ, for data measured in CECA 13X binder pellets by Cavenati et al. [10]. (a1) CO_2 (Langmuir model); (a2) CO_2 (Fowler model); (b) CH_4 (Langmuir model).

the system approaches saturation ($\theta > 0.9$) the model fails because localized models are based on the concept of a fixed number of sites with the same energy with one molecule per site. Near saturation the strong repulsion between adsorbed molecules may not satisfy the condition of uniformity of sorption sites. This drawback does not invalidate the usefulness of this simple model which can describe sorption events at molecular level in a very comprehensive and simple way.

The sorbate–sorbate interactions of CO_2 and CH_4 in Faujasite are addressed by Ghoufi et al. [46] in a molecular computational study that shows that the distance between the sorbate molecules becomes significantly shorter when the loading increases which corresponds to an increase of the CO_2–CO_2 interaction energy. It is also found in that work a significant different interaction energy between the two components with much lower values for CH_4.

Finally, with the parameters estimated from the plots in Fig. 4 and shown in Table 2 we fit the experimental isotherms measured in this work which are represented by the lines in Fig. 1. It can be seen that Fowler model for CO_2 and Langmuir model for CH_4 give a good fit. The heats of sorption obtained from the temperature dependence of parameter b according to Van't Hoff equation are also given in Table 2. They are 43.1 kJ/mol for CO_2 and 9.2 kJ/mol for CH_4 at zero coverage revealing that molecule-host crystal bonds for CO_2 are strong and low for CH_4. These results are very similar to the ones found by Mulgundmath et al. [9] and compare to 30 kJ/mol for CO_2 and 14.2 kJ/mol for CH_4 in the work of Cavenati et al. [10].

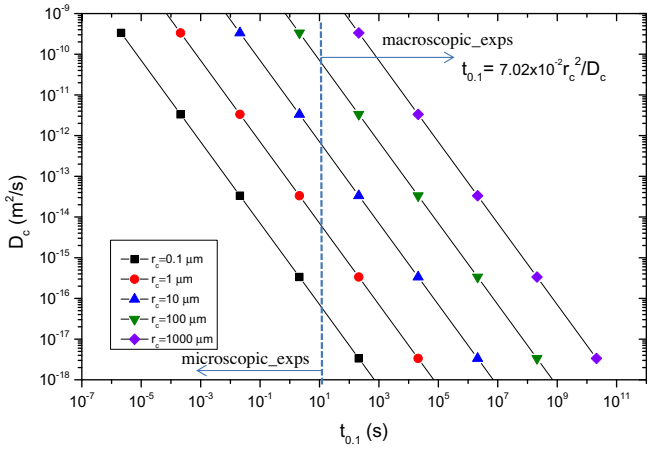

Fig. 7. Influence of different D_c (m^2/s) and r_c (μm) in the time $t_{0.1}$ (s) according to Eq. (13) that leads to a macroscopic or microscopic ZLC experiment.

4.2. Kinetics of sorption

Before doing ZLC experiments in pelletized porous adsorbents it is important to evaluate first which controlling mechanism will be dominant since there are in principle two diffusion mechanisms: the macropore diffusion representing the diffusion in the pores between zeolite beta crystals, with reciprocal time constant $D_p^2/R_p^2(1+K)$, and the micropore diffusion inside crystals with reciprocal time constant D_c/r_c^2. If diffusion mechanisms are in series Ruthven and Loughlin [47] developed a criterion to the relative importance of the diffusion mechanisms which is given by γ:

$$\gamma = \frac{D_c/r_c^2(1+K)}{D_p/R_p^2} \tag{10}$$

where $K = \rho_p H/\varepsilon_p$ and H is the dimensionless Henry's, ρ_p is the pellet density and ε_p the porosity of the pellets. Macropore diffusivity is the controlling mechanism for $\gamma > 10$; crystal diffusivity is the controlling mechanism for $\gamma < 0.1$; if $0.1 < \gamma < 10$ both macropore and micropore diffusivity should be taken into account.

In the present case it is possible to evaluate for both CO_2 and CH_4 an estimation of the controlling mechanism. For CO_2 we can read in literature [27] that diffusion in crystals is 6.4×10^{-15} m^2/s at 373 K and calculate pore diffusion for the system CO_2/He of 0.173 cm^2/s using Eq. (8) and data from Weissman et al. [48]. From the values of the Henry's constant calculated from the isotherms studies we obtain a K value of 746 using $\varepsilon_p = 0.5$. Since the size of the crystals is around 2 μm and of the beads 1.5 mm applying Eq. (10) we calculate a $\gamma = 0.085$ indicating clearly a micropore diffusion controlling mechanism. Repeating the procedure for CH_4 where: $D_c = 1 \times 10^{-9}$ m^2/s [24,26], $D_p = 0.5$ cm^2/s, $K = 19.7$, the value of γ is 236 which means a macropore diffusion control. These values guide us to understand which ZLC model (macropore or micropore) should be used in principle to calculate diffusion in the pellets of 13X zeolite for CO_2 and CH_4 by ZLC.

However, since ZLC technique is a macroscopic technique the time scale of the experiments should be preferably above 10 s. This time scale will depend of diffusion time constants. Looking at Eq. (3) that represents long time asymptotes of ZLC model from where we can get directly time constants of diffusion we can think in calculating previously the time constants for CH_4 and CO_2 to see if the study will lead to macroscopic experiments. For $L > 10$ (approximately 90% desorption curve) Eq. (3) can be further simplified to

$$\ln\left(\frac{c}{c_0}\right) = \ln\left(\frac{2}{L}\right) - \pi^2 D_c/r_c^2 t \tag{11}$$

which represented as $t = f(D_c/R_c^2)$ assumes the form,

Table 3
Experimental conditions and model parameters for ZLC experiments in binderless beads of 13X zeolite.

T (K)	Flow rate (mL/min)	−Slope (s^{-1})	Intercept	β_1	D_c/r_c^2 (s^{-1})	L
CO_2						
313	100	5.21×10^{-3}	0.5	2.35	9.43×10^{-4}*	3.37
	150	7.95×10^{-3}	0.4	2.53	1.24×10^{-3}*	4.61
					avg. 1.09×10^{-3}*	
343	60	1.51×10^{-2}	0.7	1.91	4.14×10^{-3}	1.67
	90	2.27×10^{-2}	0.5	2.35	4.12×10^{-3}	3.37
					avg. 4.13×10^{-3}	
373	30	2.70×10^{-2}	0.6	2.15	5.84×10^{-3}	2.44
	60	3.47×10^{-2}	0.4	2.53	5.43×10^{-3}	4.61
					avg. 5.64×10^{-3}	
E_a (kJ/mol)					27.0	
CH_4						
					K_{exp} (−)	K_{iso}
313	15	0.397	1.0		12.3	12.4

* These values should be read with caution since experiments where performed probably in the limit of the validity of Henry's law of isotherm.

$$t = \frac{\ln\left(\frac{(2/L)}{(c/c_0)}\right)}{\pi^2}\frac{r_c^2}{D_c}. \quad (12)$$

For $L = 10$ and $c/c_0 = 0.1$ which means 90% of the desorption curve we get,

$$t_{0.1} = 7.02 \times 10^{-2}\frac{r_c^2}{D_c}. \quad (13)$$

The previous equation can be used for a criterion to evaluate which type of systems can be measured by ZLC experiments in a macroscopic time. We remark that if we choose $L = 100$ and $c/c_0 = 0.01$ (99% of the desorption curve) or $L = 1000$ and $c/c_0 = 0.01$ (99.9%), etc., we will reach the same dimensionless constant 7.02×10^{-2}.

Fig. 7 shows the influence of the combination of crystal diffusivity (D_c) and crystal radius (r_c) that produce a macroscopic or microscopic ZLC experiment according to Eq. (13). As an example, if crystal radius of the adsorbent is 1 μm we only get a macroscopic time $t_{0.1}$ higher than 10 s if D_c is $\leqslant 1.0 \times 10^{-14}$ m^2/s, otherwise $t_{0.1}$ was $\leqslant 10$ s and ZLC desorption curve cannot be measured. As another example of application of Eq. (13), to measure a D_c of 1×10^{-10} m^2/s we will need a crystallite with $r_c \geqslant 100$ μm. It should be noted that Eq. (13) is also useful to verify if the calculated time constants of diffusion D_c/r_c^2 from the modeling of the ZLC experiments are in accordance with the predicted macroscopic experiment highlighted in Fig. 7.

For the present system since the diffusion of CO_2 reported in literature is 1.8×10^{-15} m^2/s (at 373 K) and the crystal size is 2 μm the value of $t_{0.1}$ calculated from Eq. (13) is 39 s which means that it is possible to carry out a macroscopic ZLC experiment for CO_2 in zeolite 13X. In the paper of Eic and Ruthven [29] it is remarked that ZLC experiments requires $D_c/r_c^2 < 0.01$ s^{-1}. By using Eq. (13) this means a time above 7 s. This result is validated by Eq. (13). In the case of a macropore diffusion control mechanism Eq. (13) assumes the form,

$$t_{0.1} = 7.02 \times 10^{-2}\frac{R_p^2(1+K)}{D_p}. \quad (14)$$

For CH_4 using $D_p = 0.5$ cm^2/s, $R_p = 0.075$ cm and $K = 19.7$ the value of $t_{0.1}$ is 0.016 s which means a microscopic experiment that cannot be measured by ZLC. Assuming micropore controlling mechanism for CH_4 with $D_c = 1 \times 10^{-9}$ m^2/s and 2 μm crystals we get $t_{0.1} = 7.02 \times 10^{-5}$ s a value that turns the measurement of crystal diffusivity of CH_4 by ZLC impossible unless we have crystals of at least 1000 μm (1 mm) to get $t_{0.1} = 17.5$ s. These results allow us to study the crystal diffusivity of CO_2 in 13X zeolite using ZLC experiments.

To measure D_c for CO_2, several experimental ZLC desorption runs were performed at the temperatures of 313, 343 and 373 K. Table 3 summarizes all the experiments performed including experimental conditions such as the flowrate of carrier gas and temperature. The column was saturated with a very low partial pressure around 0.01 atm that is the lowest possible for our experimental apparatus. Looking at the isotherm data this value of partial pressure assure that experiments were performed under the validity of Henry's law at 343 and 373 K, but at 313 K there is a deviation and results should be read with caution. Purge flowrates selected were high ranging from 30 mL/min to 150 mL/min to assure a kinetic regime increasing in this way the value of parameter L.

Fig. 8 shows in semi-log plots the effect of purge flowrate in the ZLC runs at the temperatures of 313 K (Fig. 8a), 343 K (Fig. 8b) and 373 K (Fig. 8c) where it can be clearly seen a long time asymptote where the intercept with the c/c_0 axis occurs at a value lower than one which means that experiments were performed under a kinetic regime. In all runs the expected proportionality between purge flowrate and parameter L is observed with a diffusional time constant practically independent of flowrate, as expected. These trends are also easily observed in Fig. 8.

Fig. 9 shows the effect of temperature in the ZLC desorption curves where it can be seen a strong temperature dependence of desorption time. The activation energy calculated from the time constants and represented in Table 3 indicates a value of 27 kJ/mol which is an expected value for crystal diffusion. It should be noted that in a macropore diffusional regime the activation energy for the apparent time constant should be in the order of the heats

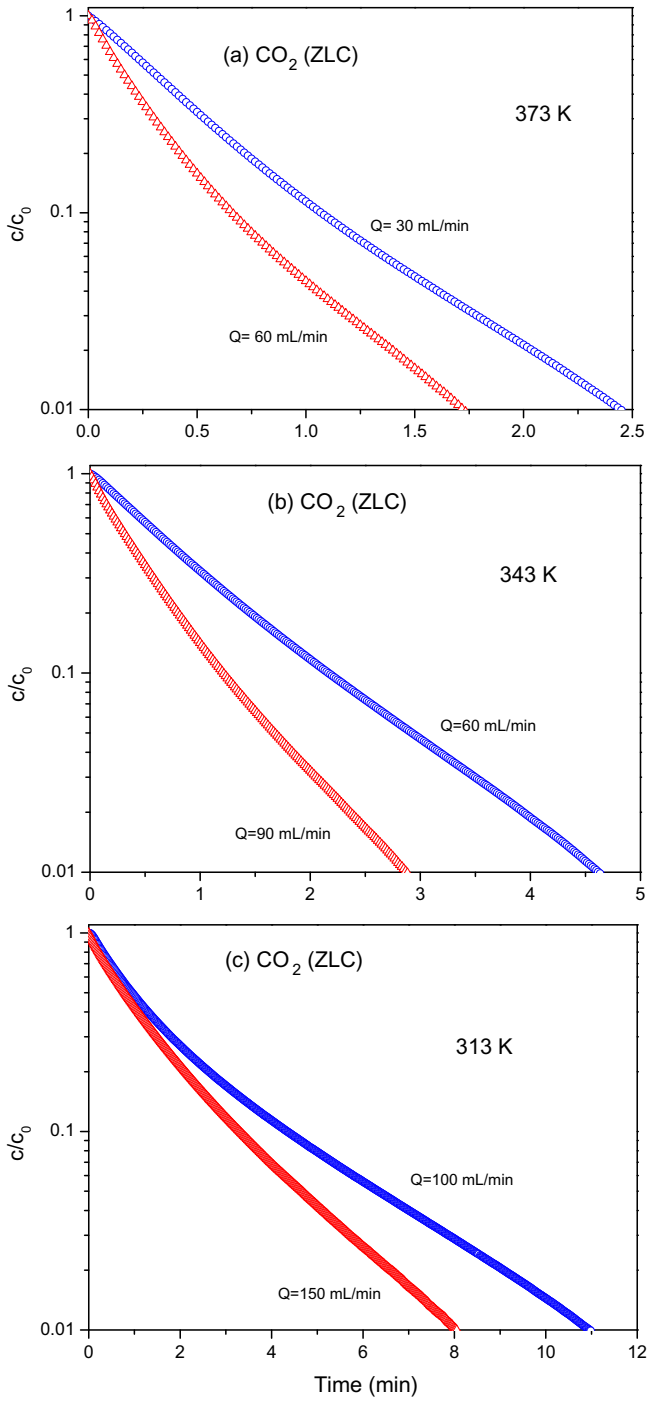

Fig. 8. Effect of flowrate on ZLC desorption curves of CO_2: (a) 373 K, (b) 343 K, (c) 313 K. Semi-log plot of c/c_0 *vs* time t.

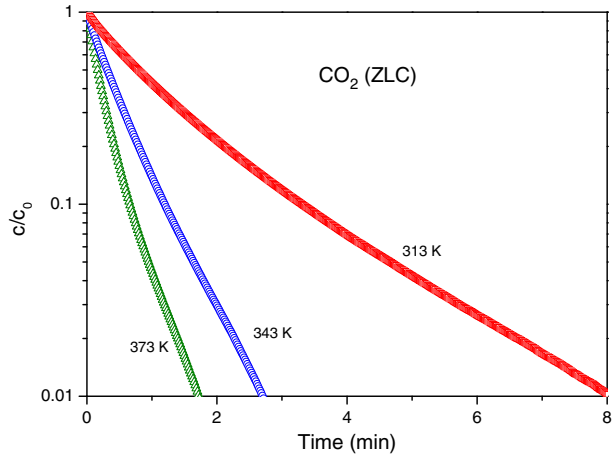

Fig. 9. Effect of temperature on ZLC desorption curves of CO_2. Semi-log plot of c/c_0 *vs* time *t*.

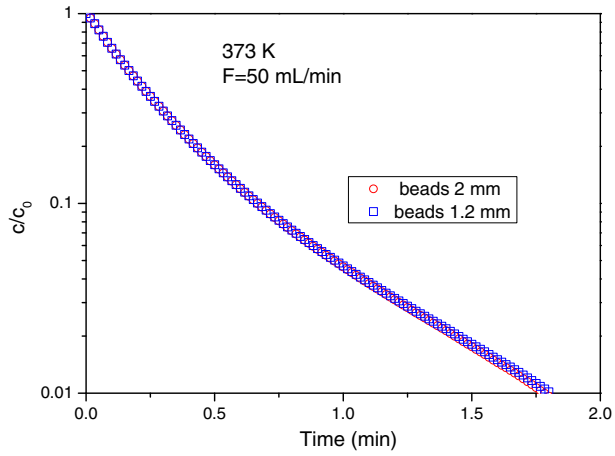

Fig. 10. Effect of beads size on ZLC desorption curves of CO_2. Semi-log plot of c/c_0 *vs* time *t*.

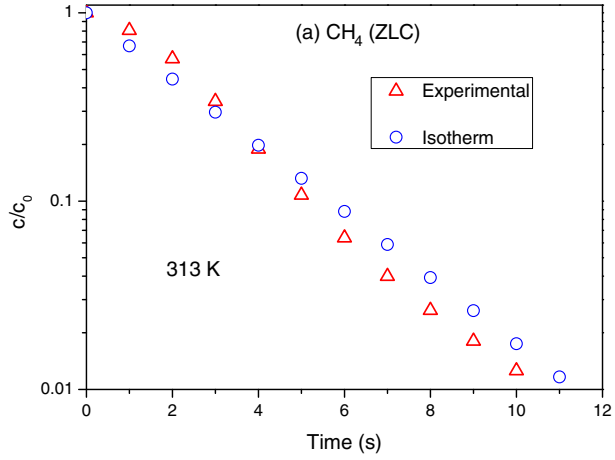

Fig. 11. ZLC desorption curves of CH_4 at 313 K and purge flowrate of 15 mL/min. Semi-log plot of c/c_0 *vs* time *t*.

of sorption where for the present case the value is 43.1 kJ/mol (see Table 2). Since the batch of the beads studied range from 1.2 mm to 2.0 mm we isolate the smaller beads from the larger ones and perform two different experiments to confirm is ZLC desorption curves are sensitive or not to the size of pellets. If they are not sensitive it means that the sorption rate is dominated crystal diffusion. Fig. 10 show the experiments performed at 373 K under a similar flowrate of 50 mL/min being clear that the size of pellets does not change the shape of the desorption curves. Accordingly, we believe that ZLC experiments were performed under a kinetic regime controlled by intracrystalline diffusivity being the values of D_c (2 μm crystal size) for CO_2 in 13X at 373 K of 5.64×10^{-15} m^2/s, at 343 K of 4.13×10^{-15} m^2/s and at 313 K 1.09×10^{-15} m^2/s. It should be noted that the value of D_c obtained in this work at 373 K compares to a value of D_c of 6.4×10^{-15} m^2/s at 373 K measured by a Frequency Response Technique [27].

For CH_4 we demonstrated previously that it is expected that kinetic data will be governed by a macropore controlling diffusion regime. However, we can evaluate if it is possible to obtain such information by ZLC. Accordingly, we can estimate previously the magnitude of parameter L for the experiments. Using Eq. (5) and data from the isotherms we calculate the value $L = 0.01$ for a purge flowrate of 10 mL/min and $L = 0.1$ for a purge flowrate ten times higher. These values indicate that ZLC experiments for CH_4 in 13X will be performed under an equilibrium regime according to Eq. (9). Fig. 11 shows the desorption curve performed at 313 K at a purge flowrate of 15 mL/min. The experiment is very fast (lower than 10 s for 99% of the desorption curve) and it is clearly seen that the intercept of the long time asymptote is 1 in the semi-log plot corresponding physically to the expected equilibrium regime. To validate this experiment we plot the predicted ZLC experiment using the isotherm data represented in Table 2 for CH_4 at 313 K. Fig. 11 shows that the experiment is validated. This means that for CH_4 diffusion data in macropores and micropores could not be measured by ZLC unless we have crystals or beads with a much bigger size. For the other temperatures of 343 and 373 K experiments are too fast that data is unreliable.

5. Conclusions

We performed a detailed study of the sorption and kinetics of CO_2 and CH_4 in binderless beads of 13X zeolite between 313 and 373 K at partial pressure up to 4 bar.

The sorption equilibrium isotherms of CO_2 are pronounced type I and show an amount adsorbed of CO_2 around 5.2 $mmol/g_{ads}$ at 4 bar which is 20% higher than values reported in literature for CECA 13X zeolite with binder. The sorption equilibrium of CO_2 was successfully modeled with the Fowler isotherm that accounts for lateral interactions between molecules adsorbed in adjacent sites. For the modeling we use a maximum capacity for sorption of CO_2 in 13X of 7.4 $mmol/g_{ads}$ measured at 32 atm and 298 K reported in literature. The CH_4 isotherms were fitted with the Langmuir model but are practically linear until 4 atm of pressure. The isosteric heat of sorption decreases linearly with coverage for CO_2 and is practically constant for CH_4.

It is demonstrated that CO_2 diffusion in crystals of 13X can be measured by ZLC in a macroscopic time using pellets or beads with crystals of 2 μm of size. However, for CH_4 that is impossible even for macropore diffusion. The diffusivity of CO_2 in 13X at 373 K measured is around 5.4×10^{-15} m^2/s which is comparable to a value reported in literature measured by a frequency response technique.

A simple equation that can be used to predict if a ZLC experiment can be performed in a macroscopic time is derived and applied for the present system proving that sorption of CO_2 in 13X zeolite can be measured macroscopically. The equation developed is also useful to check if diffusivity data calculated are consistent with a macroscopic experiment. The time of the experiments (that

should be above a few seconds) is directly related with the diffusion time constant by the following expression: $t_{0.1} \geq 7.02 \times 10^{-2} \frac{r_c^2}{D_c}$.

Acknowledgment

We acknowledge Chemiewerk Bas Kostritz GmbH (Germany) for kindly providing the samples of binderless 13X zeolite beads studied in this work.

References

[1] G. Férey, C. Serre, T. Devic, G. Maurin, H. Jobic, P.L. Llewellin, G. Weireld, A. Vimont, M. Daturi, J.S. Chang, Chem. Soc. Rev. 40 (2011) 550–562.
[2] D.M. D'Alessandro, B. Smit, Jeffrey R. Long, Angew. Chem. Int. Ed. 49 (2010) 6058–6082.
[3] H. Walter, Synthetic crystalline zeolite produced from dehydrated aluminum silicate, US Patent 3472,617, 1962.
[4] D.W. Breck, Zeolite Molecular Sieves, John Wiley & Sons, New York, 1974.
[5] K. Schumann, B. Unger, A. Brandt, F. Scheffler, Microporous Mesoporous Mater. (2011), http://dx.doi.org/10.1016/j.micromeso.2011.07.015.
[6] K.F. Loughlin, M.A. Hasanain, H.B. Abdul-Rehman, Ind. Eng. Chem. Res. 29–7 (1990) 1535–1546.
[7] Y. Wang, M.D. LeVan, J. Chem. Eng. Data 55 (2010) 3189–3195.
[8] Z. Zhang, W. Zhang, X. Chen, Q. Xi, Z. Li, Sep. Sci. Technol. 45 (2010) 710–719.
[9] V. P. Mulgundmath, F. H. Tezel, T. Saatcioglu and T. C. Golden, The, Canadian Journal of Chemical Engineering, DOI: 10.1002/cjce.20592.
[10] S. Cavenati, C.A. Grande, A.E. Rodrigues, J. Chem. Eng. Data 49 (2004) 1095–1101.
[11] P.S. Crespo, E.V.R. Fernandez, J. Gascon, F. Kapteijn, Chem. Mater. 23 (2011) 2565–2572.
[12] Z. Bao, L. Yu, Q. Ren, X. Lu, S. Deng, J. Colloid Interface Sci. 353 (2011) 549–556.
[13] Z.R. Herm, R. Krishna, J.R. Long, Microporous Mesoporous Mater. 151 (2012) 481–487.
[14] G. Férey, C. Serre, C. Mellot-Draznieks, F. Millange, S. Surblé, J. Dutour, I. Margiolaki, Angew. Chem. Int. Ed. 43 (2004) 6296–6301.
[15] L. Hamon, E. Jolimaître, G.D. Pirngruber, Ind. Eng. Chem. Res. 49 (2010) 7497–7503.
[16] S. Cavenati, C.A. Grande, A.E. Rodrigues, Ind. Eng. Chem. Res. 47 (2008) 6333.
[17] E. Stavitski, E.A. Pidko, S. Couck, T. Remy, E.J.M. Hensen, B.M. Weckhuysen, J. Denayer, J. Gascon, F. Kapteijn, Langmuir 27 (2011) 3970–3976.
[18] S. Sircar, Sep. Sci. Technol. 23 (6&7) (1988) 519–529.
[19] S. Sircar, W.C. Kratz, Sep. Sci. Technol. 23 (1998) 2397–2415.
[20] S. Cavenati, C.A. Grande, A.E. Rodrigues, Adsorption 11 (2005) 549–554.
[21] S. Cavenati, C.A. Grande, A.E. Rodrigues, Energy Fuels 19 (2005) 2545–2555.
[22] R.M. Barrer, Zeolites and Clay Minerals as Sorbents and Molecular Sieves, Academic Press, London, 1978.
[23] D.M. Ruthven, Principles of Adsorption and Adsorption Processes, John Wiley & Sons, New York, 1984.
[24] G. Guiochon, S.G. Shirazi, A.M. Katti, Fundamentals of Preparative and Nonlinear Chromatography, Academic Press, London, 1994.
[25] D. D. Do, Adsorption analysis: equilibria and kinetics, Imperial College Press, 1998.
[26] J. Karger, D.M. Ruthven, Diffusion in Zeolites and Others Microporous Solids, John Wiley & Sons, New York, 1992.
[27] G. Onyestyák, L.V.C. Rees, J. Phys. Chem. B 103 (1999) 7469–7479.
[28] J. Guo, D.B. Shah, O. Talu, Ind. Eng. Chem. Res. 46 (2007) 600–607.
[29] M. Eic, D.M. Ruthven, Zeolites 8 (1988) 40–45.
[30] S. Brandani, J.R. Hufton, D.M. Ruthven, Zeolites 15 (1995) 624–631.
[31] C.L. Cavalcante, D.M. Ruthven, Ind. Eng. Chem. Res. 34 (1995) 177.
[32] C.L. Cavalcante, D.M. Ruthven, Ind. Eng. Chem. Res. 34 (1995) 184.
[33] P.M. Lima, C.V. Gonçalves, C.L. Cavalcante, D. Cardoso, Microporous Mesoporous Mater. 116 (2008) 352–357.
[34] P.S. Bárcia, J.A.C. Silva, A.E. Rodrigues, Microporous Mesoporous Mater. 79 (2005) 145–163.
[35] D.M. Ruthven, P. Stapleton, Chem. Eng. Sci. 48 (1993) 89–98.
[36] S. Brandani, D.M. Ruthven, Chem. Eng. Sci. 50 (1995) 2055–2059.
[37] J.A.C. Silva, A.E. Rodrigues, Ind. Eng. Chem. Res 36 (1997) 493–500.
[38] S. Brandani, C.L. Cavalcante, A.M. Guimarães, D.M. Ruthven, Adsorption 4 (1998) 275–285.
[39] J.A.C. Silva, F.A. Da Silva, A.E. Rodrigues, Ind. Eng. Chem. Res. 40 (2001) 3697–3702.
[40] S. Brandani, Chem. Eng. Sci. 53 (1998) 2791–2798.
[41] D.M. Ruthven, F. Brandani, Adsorption 11 (2005) 31–34.
[42] D.M. Ruthven, A. Vidoni, Chem. Eng. Sci. 71 (2012) 1–4.
[43] F. Brandani, D.M. Ruthven, C.G. Coe, Ind. Eng. Chem. Res. 42 (2003) 1451–1461.
[44] P.S. Bárcia, J.A.C. Silva, A.E. Rodrigues, Ind. Eng. Chem. Res. 45 (2006) 4316–4328.
[45] R.H. Fowler, E.A. Gugghenheim, Statistical Thermodynamics, Cambridge University Press, Cambridge, UK, 1939.
[46] A. Ghoufi, L. Gaberova, J. Rouquerol, D. Vincent b, P.L. Llewellyn, G. Maurin, Microporous Mesoporous Mat. 119 (2009) 117–128.
[47] D.M. Ruthven, K.F. Loughlin, Can. J. Chem. Eng. 50 (1972) 550.
[48] S. Weissman, S.C. Saxena, E.A. Mason, Phys. Fluids 3 (510) (1960) 510–518.